Early Universe Neutrino Oscillations

Michelle Thran*
Physics Department, University of Chicago

Vincenzo Cirigliano†
Institute of Nuclear Theory
Senior Fellow, Professor
(Dated: December 15, 2023)

In this paper, we implement a toy model of early universe (EU) neutrino flavor oscillations in the 30 MeV $\rightarrow$ 1 MeV temperature regime with the goal of modeling the netrino flavor and energy spectra in the moments before neutrino decoupling. The model utilizes an effective Hamiltonian with e^+e^- and $\nu\bar{\nu}$ thermal interactions and neutrino lepton number potentials, and tracks both coherent flavor oscillations and decohering flavor-dependent inelastic collisions. We find that neutrinos and antineutrinos both decouple as mass-aligned states and maintain a Fermi-Dirac energy distribution. When the neutrino lepton potential is omitted, both neutrinos and antineutrinos born electron-flavored decouple as non-electron flavored. The neutrino lepton number potential induces strong differences between the end flavor spectrum of neutrinos and antineutrinos, and its inclusion in the model causes either neutrinos or antineutrinos to "switch back" and decouple as electron-flavored.

I. INTRODUCTION

In the moments following the Big Bang, the rapidly cooling and expanding early universe was composed of matter and radiation in thermal equilibrium. Neutrinos decoupled at $\sim$ 1 s , leaving behind a cosmic neutrino background (CνB) analogous to the cosmic background microwave radiation released after photon-decoupling. These so-called "relic neutrinos" still exist today but, with temperatures estimated to be on the order of $\sim 10^{-4} - 10^{-6}$ eV, have not yet been directly observed [1]. Much is unknown about these neutrinos. This paper aims to address the question of the energy spectrum and flavor content of these neutrinos following their decoupling. This information has wide implications: Firstly, the neutron-proton ratio at the time of Big Big Nucleosynthesis (BBN) is dependent on the abundance of electron-flavor neutrinos and antineutrinos. Secondly, the impact of inelastic collisions on neutrino propagation is relevant for cosmological neutrinos more generally; for example, the neutrinos scattered during supernovae are subject to significant inelastic collisions with the medium.

In the interest of being "self-contained", this paper begins with an introduction to neutrinos, neutrino oscillations, and early universe cosmology. We hope to provide relevant background information while assuming as little prior knowledge as possible. We then walk through a description and derivation of the quantum kinetic equations (QKEs) used (section II). Detailed descriptions of our findings are given in section III.

A. Background: Neutrinos and Neutrino Oscillations

Neutrinos are electrically neutral fermions that interact with other particles through the weak interaction and gravity. Although initially believed to be massless, neutrinos are now understood to have three definite-mass eigenstates $|\nu_i\rangle, i = 1, 2, 3$ [2]. These masses are not precisely known. Participation in the weak interaction produces neutrinos in one of three flavors, $|\nu_\alpha\rangle, \alpha = e, \mu, \tau$. Curiously, a neutrino's flavor may change as the neutrino propagates; a neutrino born as an $\alpha-$neutrino may later be observed as a $\beta-$neutrino. This phenomenon, called "neutrino oscillation" has great historical significance and has been taken as strong evidence that neutrinos have nonzero mass.

Neutrinos of definite flavor are related to neutrinos of definite mass according to the relation $|\nu_\alpha\rangle = \sum_i U^*_{\alpha i} |\nu_i\rangle$, where $U \in U(3)$ is the flavor-mixing matrix. The statement that $U_{\alpha i} \neq I$ (i.e., that definite-flavor neutrinos do not coincide with definite-mass neutrinos) provides the mechanism for neutrino oscillation. As a neutrino of a definite-flavor $|\nu_\alpha\rangle$ propagates, the phases for each of the constituent mass eigenstates evolve differently: the time-dependent Schrödinger equation gives the evolution of each mass eigenstate with respect to proper time τ_i:

$$i\frac{\partial}{\partial\tau_i}|\nu_i(\tau_i)\rangle = m_i|\nu_i(\tau_i)\rangle$$
$$\implies |\nu_i(\tau_i)\rangle = e^{-im_i\tau_i}|\nu_i\rangle$$

Neutrinos are extremely light, therefore we use the relativistic approximation and set $p_i = \sqrt{E_i^2 - m_i^2} \approx E_i - m_i^2/2E_i$, where p_i and E_i are momentum and energy in lab frame. Now $m_i\tau_i = (E_i t - p_i L)$ (where $t \approx L$ are time and length in lab frame) may be approximated as $m_i\tau_i \approx m_i^2 t/2E_i$. Therefore we have

$$|\nu_i(t)\rangle \approx e^{-m_i^2 t/2E_i}|\nu_i\rangle$$

* micthran@gmail.com
† https://phys.washington.edu/people/vincenzo-cirigliano

Which gives

$$\langle \nu_\beta | \nu_\alpha(t) \rangle = \left[\sum_j \langle \nu_j | U_{\beta j} \right] \left[\sum_i U^*_{\alpha i} | \nu_i(t) \rangle \right] \approx \sum_i U_{\beta i} U^*_{\alpha i} e^{-m_i^2 t/2E_i} \neq 0$$

Thus the probability that a neutrino oscillates from flavor α to flavor β is nonzero.

Neutrino propagation can be analyzed using the effective Hamiltonian formalism. The vacuum effective Hamiltonian H_V is determined by the flavor-mixing matrix U and (in the flavor basis) has components:

$$[H_V]_{\alpha\beta} = \langle \nu_\alpha | H_V | \nu_\beta \rangle = \sum_i \sum_j U_{\alpha i} U^*_{\beta j} \langle \nu_i | H_V | \nu_j \rangle = \sum_i U_{\alpha i} U^*_{\beta i} E_i$$

Let

$$U = \begin{bmatrix} \cos\theta_V & \sin\theta_V \\ -\sin\theta_V & \cos\theta_V \end{bmatrix}$$

for some flavor-mixing angle θ_V. Plugging this form for U in directly into the expression for H_V yields a rather unwieldy form for H_V. It can be made nicer by recognizing that adding any scalar multiple of the identity matrix does not change the final probability amplitudes. By making a clever choice $C = -p + \left(m_1^2 - m_2^2\right)/4p$ (where m_1 is defined to be the heavier of the two masses) then, skipping over the algebra (see [3] for a more comprehensive derivation),

$$H'_V = H_V + CI = \frac{\Delta m^2}{4E} \begin{bmatrix} -\cos 2\theta_V & \sin 2\theta_V \\ \sin 2\theta_V & \cos 2\theta_V \end{bmatrix}$$

This is the form that is generally used for the "vacuum effective Hamiltonian", H_V.

Deviations from the vacuum Hamiltonian lead to different energy eigenstates and therefore different oscillation probabilities. As an example, consider neutrinos in the presence of matter. Matter generally consists of electrons and nucleons which, through $W-$ and $Z-$boson exchanges, induce elastic forward scattering. In the Mikheyev-Smirnov-Wolfenstein (MSW) effect, solar electrons interact with electron-neutrinos via W-exchange, which leads to matter potential $V_W = \sqrt{2} G_F N_e |\nu_e\rangle \langle \nu_e|$ (where G_F is the Fermi coupling constant and N_e is the electron density; see [4] for a derivation) [3, 5]. $Z-$exchange also induces neutrino scattering in the sun, but because the scattering amplitudes are the same for all three neutrino flavors, the corresponding matter potential V_Z is a scalar multiple identity in the flavor basis and therefore does not contribute to the overall probability of flavor oscillation.

B. Background: Early Universe Cosmology

This subsection gives a (very!) brief description of early universe (EU) cosmology, particularly the aspects relevant to relic neutrinos. In this section, we assume that our system is described by the "perfect fluid" stress-energy tensor:

$$T_{ab} = \rho u_a u_b + P\left(g_{ab} + u_a u_b\right)$$

where u^a is four-velocity, ρ is energy density, and P is pressure. Indeed, if we assume the universe is isotropic (no preferred spatial direction) and homogeneous on the cosmic scale, then the "perfect fluid" form is actually the most general possible form for T_{ab} [6]. The dynamics of our homogeneous and isotropic universe may be divided broadly into three regimes (listed in temporal order; see [1] for more details):

- **"radiation dominated"**: The "radiation dominated" universe has its energy density dominated by massless (or near massless) particles such as photons and neutrinos. The equation of state for massless thermal radiation has pressure given by $P_R = \rho_R/3$
- **"matter dominated"**: The "matter dominated" or "dust-filled" universe has most of its mass-energy coming from "ordinary matter" (i.e., non-relativistic particles). The motion of matter is small, therefore pressure P_M is taken to be negligible.
- **"vacuum dominated"**: Under the Λ-CDM model of cosmology, a cosmological constant Λ is inserted into Einstein's equation to accommodate dark energy. This constant has the effect of "negative pressure", therefore we take $P_\Lambda = -\rho_\Lambda$

The assumptions of homogeneity and isotropy require that the spatial geometry of the universe be a space of constant curvature [6]. This is described by the Friedmann-Lemaître-Robertson-Walker (FLRW) metric:

$$ds^2 = dt^2 - a^2(t)\left(\frac{dr^2}{1-kr^2} + r^2 d\theta^2 + r^2 \sin^2\theta d\phi^2\right)$$

where $k = +1$ describes an open universe, $k = -1$ describes a closed universe, and $k = 0$ describes a flat universe. Using the stress-energy tensor T_{ab} and metric as they are given above, it can be shown (see [7]) that Einstein's equation

$$G_{ab} + \Lambda g_{ab} = 8\pi T_{ab}$$

produces the following evolution equations for our cosmology:

$$\frac{\dot{a}^2}{a^2} = \frac{8\pi\rho}{3} - \frac{k}{a^2}$$

$$\frac{\ddot{a}}{a} = -\frac{4\pi}{3}(\rho + 3P) + \frac{\Lambda}{3}$$

Immediately it is clear that the scale factor $a(t)$ cannot be a constant. Indeed, with the cosmological constant Λ, these equations give $\dot{a}(t), \ddot{a}(t) > 0$, indicating that the universe is expanding (and accelerating in its expansion!). The constant $\dot{a}/a \equiv H$ is known as Hubble's constant. If we assume that these expressions are true for the entire history of the universe, then we can follow them back in time and come to the conclusion that the universe was once infinitesimally small. This is the basis for the "Big Bang" model of cosmology.

The very first moments of the universe (i.e. before the end of the inflationary period, $\sim 10^{-32}$ seconds after the universe was born) are largely unknown and up to speculation. However, it is believed that the universe began as a hot and dense ($T, \rho \to \infty$) "soup" of radiation and matter in thermal equilibrium. As the universe expanded and cooled, various particles "thermalized" in stages, decoupling from the rest of the primordial material. This thermalization occurs when the particle's interaction rate Γ becomes smaller than the rate of change of the temperature; qualitatively, this corresponds to when the mean free path of a particle ($\sim \Gamma^{-1}$) is larger than the particle horizon ($\sim H^{-1}$ in the radiation-dominated universe) [1, 6]. After thermalizing, the number of decoupled particles in a (comoving) volume element remains constant, but the number density scales as $a(t)^{-3}$ (consistent with "matter dominated" regime). In the 1 MeV $\leq T \leq$ 100 MeV temperature range of the early universe, neutrinos are locked in thermal equilibrium through the weak interactions

$$\nu + \bar{\nu} \leftrightarrow e^+ + e^- \quad , \quad \overset{(-)}{\nu} + e^{\pm} \leftrightarrow \overset{(-)}{\nu} + e^{\pm}$$

which have an average cross section of $\langle \sigma v \rangle \sim G_F^2 T^2$ (where $v \approx 1$ is the neutrino velocity). The number density of relativistic particles in this regime is $n \sim T^3$ [1], therefore the interaction rate for neutrinos is

$$\Gamma = n \langle \sigma v \rangle \sim G_F^2 T^5$$

Using $H \sim T^2/M_P$ for Planck mass M_P, neutrino decoupling occurs when $\Gamma \sim H$, or

$$T_{\nu\text{-decoupling}} \sim \left(\frac{1}{M_P G_F^2} \right)^{1/3} \approx 1 \text{ MeV}$$

II. DESCRIPTION OF QKES

The simplified QKEs used in this model have the following key features:

- We work in the temperature range $T : 30$ MeV $\to$ 1 MeV , where the only thermalized relativistic particles (besides neutrinos and antineutrinos) are photons, electrons, and positrons.
- We assume two neutrino flavors ν_e and ν_x and we neglect spin degrees of freedom.
- We include a "thermal potential" which includes e^+e^- and $\nu - \bar{\nu}$ effects.
- We include neutrino lepton number effects and allow neutrinos and antineutrinos to have slightly different initial distributions. The latter effect is incorporated by introducing a small chemical potential μ in the Fermi-Dirac initial conditions.
- We include collision terms which account for processes such as $\nu_\alpha + N \leftrightarrow \nu'_\alpha + N'$. In the temperature range we are interested in, the target particles N may be electrons or positrons. These interactions may be flavor-dependent.
- We assume a non-degenerate bath of neutrinos and target particles. This allows Pauli-blocking to be neglected.
- We ignore charged lepton number (i.e. matter) effects

A. QKEs

Starting with the density matrix in flavor-basis

$$\rho = \sum_n p_n \left|\psi_n\right\rangle \left\langle\psi_n\right| \equiv \begin{bmatrix} f_{ee} & f_{ex} \\ f_{xe} & f_{xx} \end{bmatrix}$$

In the absence of inelastic collisions, the density matrix evolves according to $\frac{\partial}{\partial t}\rho = -i\left[H, \rho\right]$, where H is the "effective Hamiltonian" of the system. Introducing collision terms $C(E)$ gives the basic QKE we are interested in:

$$\frac{\partial \rho(E)}{\partial t} = -i\left[H(E), \rho(E)\right] + C(E) \tag{1}$$

Where the $H(E)$ may be split into vacuum Hamiltonian, H_V, and thermal potential $H_T(E)$:

$$H(E) = \omega(E) H_V + H_T(E) + H_L(E) \tag{2}$$

$$H_V(E) = \begin{bmatrix} -\cos 2\theta_V & \sin 2\theta_V \\ \sin 2\theta_V & \cos 2\theta_V \end{bmatrix} \tag{3}$$

$$\omega(E) = \frac{\Delta m^2}{4E} \tag{4}$$

$$H_T(E) = h_T(E) \begin{bmatrix} 1 & 0 \\ 0 & 0 \end{bmatrix} + \frac{h_T(E) \cos^2\theta_W}{2} \frac{60}{7\pi^4} \int_0^\infty d\bar{E}' \bar{E}'^3 \left(\rho(\bar{E}') + \bar{\rho}(\bar{E}') \right) \tag{5}$$

$$h_T(E) = -\frac{28\pi \sin^2\theta_W}{45\alpha} \frac{E}{T} \tag{6}$$

$$H_L(E) = \frac{G_F}{\sqrt{2}\pi^2} \int_0^\infty d\bar{E}' \bar{E}'^2 \left(\rho(\bar{E}') - \rho(\bar{E}') \right) \tag{7}$$

Where θ_V is the vacuum neutrino flavor mixing angle, Δm^2 is the difference between the two squared mass eigenvalues, θ_W is the weak mixing angle, and $\bar{E} \equiv E/T$.

The two terms of the thermal potential (equation 28) are the electron-positron and neutrino-antineutrino contributions, respectively.

The collision term $C(E)$ accounts for neutrino-electron (positron) collisions with flavor-dependent scattering amplitudes. To accommodate flavor-dependent interactions, we introduce the matrix

$$Y = \begin{bmatrix} y_e & 0 \\ 0 & y_x \end{bmatrix} \tag{8}$$

and define

$$\delta \equiv \frac{y_e - y_x}{y_e + y_x}$$

δ characterizes the degree to which the collisions vary by flavor; $\delta = 0$ corresponds to "flavor blind" collisions. The collision term is given by

$$C(E) = -\int_0^\infty dE' E'^2 K(E,E') \Big(\{Y\,(1-\rho(E'))\,Y, \rho(E)\} - e^{-(E'-E)/T} \{Y\rho(E')Y, 1-\rho(E)\} \Big)$$

where $K(E,E')$ is the collision kernel. Note that $C(E)$ includes "gain" and "loss" terms. Dropping Pauli-blocking, this simplifies to

$$C(E) = -\int_0^\infty dE' E'^2 K(E,E') \Big(\{Y^2, \rho(E)\} - e^{-(E'-E)/T} 2Y\rho(E')Y \Big) \tag{9}$$

For the antineutrino, we use the convention $\bar{\omega}(E) = -\omega(E)$ and $\bar{H}_T(E) = -H_T(E)$. The QKE for antineutrinos is therefore given by

$$\frac{\partial}{\partial t}\bar{\rho}(E) = i\left[\bar{H}(E), \bar{\rho}(E)\right] + \bar{C}(E) \tag{10}$$

Where $\bar{C}(E)$ is as above (equation 9), but with $\bar{\rho}$ replacing ρ and

$$\bar{H}(E) = -\omega(E) H_V - H_T(E) + H_L(E) \tag{11}$$

. Note that the matter potential term H_L keeps the same sign as in the neutrino Hamiltonian.

B. Bloch Formalism

Any Hermitian matrix may be written in terms of the Pauli matrices, therefore we define

$$\rho = \frac{1}{2}\left(P_0 I + \vec{P}\cdot\vec{\sigma}\right), \quad \bar{\rho} = \frac{1}{2}\left(\bar{P}_0 I + \vec{\bar{P}}\cdot\vec{\sigma}\right) \tag{12}$$

$$H = \frac{1}{2}\left(B_0 I + \vec{B}\cdot\vec{\sigma}\right), \quad \bar{H} = \frac{1}{2}\left(\bar{B}_0 I + \vec{\bar{B}}\cdot\vec{\sigma}\right) \tag{13}$$

It is worth taking a minute to appreciate the physical significance of this construction. Recall that the diagonal elements of the density matrix ρ represent the populations of each flavor. In the $(I, \sigma_x, \sigma_y, \sigma_z)$ basis, diagonal matrix entries are $1+\sigma_z$ and $1-\sigma_z$, respectively, therefore the σ_z-components of $\vec{P}$ and $\vec{B}$ characterize the flavor-alignment of the system (We are not concerned with the identity term I because multiples of I do not contribute to the commutator). For example, $P_z = P_0$ implies $f_{ee} = 1$ and $f_{xx} = 0$, while $P_z = -P_0$ implies $f_{ee} = 0$ and $f_{xx} = 1$. Plugging equations 12 and 13 directly into equation 1 yields

$$\frac{\partial}{\partial t}P_0 = C_0(E) \tag{14}$$

$$\frac{\partial}{\partial t}\vec{P} = \left(\omega(E)\hat{B}_V + \vec{B}_T(E) + \vec{B}_L(E)\right) \times \vec{P} + \vec{C}(E) \tag{15}$$

$$\frac{\partial}{\partial t}\bar{P}_0 = \bar{C}_0(E) \tag{16}$$

$$\frac{\partial}{\partial t}\vec{P} = \left(-\omega(E)\hat{B}_V - \vec{B}_T(E) + \vec{B}_L(E)\right) \times \vec{P} + \vec{\bar{C}}(E) \tag{17}$$

where

$$\hat{B}_V = \begin{pmatrix} \sin 2\tilde{\theta} \\ 0 \\ \cos 2\tilde{\theta} \end{pmatrix}; \quad \omega(E) = \frac{\Delta m^2}{2E}; \quad \tilde{\theta} = \frac{\pi}{2} - \theta_V \tag{18}$$

$$\vec{B}_T(E) = h_T(E) \begin{pmatrix} 0 \\ 0 \\ 1 \end{pmatrix} + h_T \frac{\cos^2(\theta_W)}{2} \frac{60}{7\pi^4} \int_0^\infty d\bar{E}' \bar{E}'^3 \left[\vec{P}(\bar{E}') + \vec{\bar{P}}(\bar{E}')\right] \tag{19}$$

$$\vec{B}_L(E) = \frac{G_F}{\sqrt{2}\pi^2} \int_0^\infty d\bar{E}' \bar{E}'^2 \left[\vec{P}(\bar{E}') - \vec{\bar{P}}(\bar{E}')\right] \tag{20}$$

$$C_0(E) = -\frac{1}{2}(y_e + y_x)^2 \int_0^\infty dE' E'^2 K(E,E') \times \Big[(1+\delta^2)\left(P_0(E) - e^{\frac{E'-E}{T}} P_0(E')\right) + 2\delta\left(P_z(E) - e^{\frac{E'-E}{T}} P_z(E')\right)\Big] \tag{21}$$

$$\vec{C}(E) = -\frac{1}{2}(y_e + y_x)^2 \int_0^\infty dE' E'^2 K(E,E') \times \Big[\hat{x}\left((1+\delta^2)P_x(E) - (1-\delta^2)e^{\frac{E'-E}{T}} P_x(E')\right) + \hat{y}\left((1+\delta^2)P_y(E) - (1-\delta^2)e^{\frac{E'-E}{T}} P_y(E')\right) + \hat{z}\Big((1+\delta^2)\left(P_z(E) - e^{\frac{E'-E}{T}} P_z E'\right) + 2\delta\left(P_0(E) - e^{\frac{E'-E}{T}} P_0(E')\right)\Big)\Big] \tag{22}$$

and $\bar{C}_0(E), \vec{\bar{C}}(E)$ defined similarly to equations 21 and 22, but with $\bar{P}$ swapped for P.

The form of equation 15 allows us to interpret the Hamiltonian as an effective magnetic field influencing the polarization vector $\vec{P}$. When the processes are "sufficiently adiabatic", $\vec{P}$ precesses about $\vec{B}$. As we shall show below, at a high temperature, the thermal term $\vec{B}_T$ dominates, which causes $\vec{B}$ to align with $\hat{\sigma}_z$ ("flavor

alignment"). As the temperature decreases, the vacuum term $\hat{B}(E)$ eventually dominates.

C. n Energy bins

We can further simplify the above system of equations by replacing the continuum $E \in (0, \infty)$ with n bins of width ΔE centered at $E_1, \cdots, E_n$. For brevity, we will write $\vec{P}(E_i) \equiv \vec{P}_i, \omega(E_i) \equiv \omega_i$, etc. We also replace the collision kernel $K(E, E')$ with a matrix

$$g_{ij} = \frac{1}{2}(y_e - y_x)^2 \Delta E \; K(E_i, E_j) E_j^2 \tag{23}$$

which will be populated with numeric values $g_{ij} \propto E_j^2/(|E_i - E_j| + 1)$. With these replacements, equations 14 through 22 become

$$\frac{\partial}{\partial t} P_{0,i} = C_{0,i} \tag{24}$$

$$\frac{\partial}{\partial t} \vec{P}_i = \left(\omega_i \hat{B}_V + \vec{B}_{T,i} + \vec{B}_{L,i}\right) \times \vec{P}_i + \vec{C}_i \tag{25}$$

$$\frac{\partial}{\partial t} \bar{P}_{0,i} = \bar{C}_{0,i} \tag{26}$$

$$\frac{\partial}{\partial t} \vec{\bar{P}}_i = \left(-\omega_i \hat{B}_V - \vec{B}_{T,i} + \vec{B}_{L,i}\right) \times \vec{\bar{P}}_i + \vec{\bar{C}}_i \tag{27}$$

$$\vec{B}_{T,i} = h_{T,i} \begin{pmatrix} 0 \\ 0 \\ 1 \end{pmatrix} + h_{T,i} \frac{\cos^2(\theta_W)}{2} \frac{60}{7\pi^4} \sum_k \Delta\bar{E} \; \bar{E}_k^3 \left[\vec{P}(\bar{E}_k) + \vec{\bar{P}}(\bar{E}_k)\right] \tag{28}$$

$$\vec{B}_{L,i} = \frac{G_F}{\sqrt{2}\pi^2} \sum_k \Delta\bar{E} \; \bar{E}_k^2 \left[\vec{P}(\bar{E}_k) - \vec{\bar{P}}(\bar{E}_k)\right] \tag{29}$$

$$C_{0,i} = -\sum_{k \neq i} g_{ik} \Big[(1+\delta^2)\left(P_{0,i} - e^{\frac{E_k - E_i}{T}} P_{0,k}\right) + 2\delta\left(P_{z,i} - e^{\frac{E_k - E_i}{T}} P_{z,k}\right)\Big] \tag{30}$$

$$\vec{C}_i = \hat{x}\Big(- 2g_{ii}\delta^2 P_{x,i} - \sum_{k \neq i} g_{ik}\Big[(1+\delta^2)P_{x,i} - (1-\delta^2)e^{\frac{E_k - E_i}{T}} P_{x,k}\Big]\Big) + \hat{y}\Big(- 2g_{ii}\delta^2 P_{y,i} - \sum_{k \neq i} g_{ik}\Big[(1+\delta^2)P_{y,i} - (1-\delta^2)e^{\frac{E_k - E_i}{T}} P_{y,k}\Big]\Big) + \hat{z}\Big(-\sum_{k \neq i} g_{ik}\Big[(1+\delta^2)\left(P_{z,i} - e^{\frac{E_k - E_i}{T}} P_{z,k}\right) + 2\delta\left(P_{0,i} - e^{\frac{E_k - E_i}{T}} P_{0,k}\right)\Big]\Big) \tag{31}$$

$\bar{C}_{0,i}$ and $\vec{\bar{C}}_i$ are defined similarly. This construction also has the benefit of formalizing the distinction between "weakly" versus "strongly" coupled regimes; because g_{ij} for $j \neq i$ controls the coupling between neutrinos in the energy bins E_i and E_j (see equations 30 and 31), we say the system is "strongly coupled" when $g_{ij}/\omega_k \ll 1$ and conversely is "weakly coupled" when $g_{ij}/\omega_k \gg 1$. As we shall show below, these QKEs with EU parameters are generally in the weak coupling regime.

D. Early Universe

To model the EU system, we begin by rescaling our collision matrix to be consisent with early neutrino collision rates (see I B)

$$\bar{g}_{ij} \to g_{ij} = G_F^2 T^5 \bar{g}_{ij} \tag{32}$$

where $\bar{g}_{ij}$ denotes the form given in equation 23. We similarly rescale

$$\bar{h}_{T,i} \to h_{T,i} = G_F^2 T^5 \bar{h}_{T,i} \tag{33}$$

where $\bar{h}_{T,i}$ denotes the form given in equation 6. Time evolution along a neutrino's worldline is given by the the differential

$$\frac{D}{Dt} \equiv \frac{\partial}{\partial t} - Hp\frac{\partial}{\partial p} \tag{34}$$

where $p \equiv |\vec{p}|$. Note that the assumption of spatial homogeneity has been used to drop the advection term. To simplify this, we switch to coordinates $\bar{t}$ and $\bar{p}$, where

$$\bar{t} = \frac{T_0}{T} \qquad \bar{p} = \frac{p}{T} \tag{35}$$

Where T_0 is some arbitary constant. For convience, we take $T_0 = 1$ MeV. In the radiation-dominated era, $T^{-1}, p^{-1} \propto a(t)$, therefore, after making the substitution, D/Dt can be rewritten as

$$\frac{D}{Dt} \to \bar{t} H \frac{\partial}{\partial \bar{t}} \tag{36}$$

Here (again consistent with the radiation-dominated era, and neglecting contributions from nonrelativistic particles) we take Hubble's constant to be

$$H = \frac{h T_0^2}{M_P} \cdot \frac{1}{\bar{t}^2} \tag{37}$$

where

$$h = \left(\frac{4\pi^3 g_\rho}{45}\right)^{1/2} \tag{38}$$

g_ρ sums over the contributions of all relativistic particles. In the temperature range we are concerned with (1 MeV $\leq T \leq$ 30 MeV), the thermalized relativistic particles are $\gamma, e^\pm, \nu, \bar{\nu}$, which gives $g_\rho = 43/4 = 10.75$ [1].

Now, interpreting $\partial/\partial t$ in the previous sections to be D/Dt, we divide the RHS of equations 24 through 31 by $\bar{t}H$. This amounts to transforming

$$\omega_i \to \omega_i(\bar{t}) = \frac{1}{\bar{t}H}\omega_i$$
$$= \left(\frac{M_P}{hT_0^3}\right)\bar{\omega}_i\bar{t}^2 \approx 0.2243\times10^{10}\ \bar{\omega}_i\bar{t}^2 \quad (39)$$
$$h_{T,i} = G_F^2T^5\bar{h}_{T,i} \to \frac{1}{\bar{t}H}\bar{h}_{T,i}G_F^2T^5$$
$$= \frac{M_PT_0^3G_F^2}{h}\bar{h}_{T,i}\cdot\frac{1}{\bar{t}^4} \approx 0.30519\ \bar{h}_{T,i}\cdot\frac{1}{\bar{t}^4} \quad (40)$$
$$g_{ij} = G_F^2T^5\bar{g}_{ij} \to \frac{1}{\bar{t}H}\bar{g}_{ij}G_F^2T^5$$
$$= \frac{M_PT_0^3G_F^2}{h}\bar{g}_{i,j}\cdot\frac{1}{\bar{t}^4} \approx 0.30519\ \bar{g}_{ij}\cdot\frac{1}{\bar{t}^4} \quad (41)$$
$$\frac{G_F}{\sqrt{2}\pi^2} \to \frac{1}{\bar{t}H}\frac{G_F}{\sqrt{2}\pi^2}$$
$$= \frac{M_PT_0G_F}{h\sqrt{2}\pi^2}\frac{1}{\bar{t}^2} \approx 1.874\times10^9\frac{1}{\bar{t}^2} \quad (42)$$

where $\bar{\omega}_i$ is defined similar to the form given in equation 18, but with $E \to E_i/T$.

Inserting equations 39 through 41 into the QKEs as they appear in equations 24 through 31 gives the final form of the QKEs used in our model:

$$\frac{\partial}{\partial\bar{t}}P_{0,i} = \left(\frac{M_PT_0^3G_F^2}{h}\frac{1}{\bar{t}^4}\right)C_{0,i} \quad (43)$$
$$\frac{\partial}{\partial\bar{t}}\vec{P}_i = \left[\left(\frac{M_P}{hT_0^3}\bar{\omega}_i\bar{t}^2\right)\hat{B}_V + \left(\frac{M_PT_0^3G_F^2}{h}\frac{\bar{h}_{T,i}}{\bar{t}^4}\right)\vec{B}_{T,i} + \left(\frac{M_PT_0G_F}{h\sqrt{2}\pi^2}\frac{1}{\bar{t}^2}\right)\vec{B}_{L,i}\right]\times\vec{P}_i + \left(\frac{M_PT_0^3G_F^2}{h}\frac{1}{\bar{t}^4}\right)\vec{C}_i \quad (44)$$
$$\frac{\partial}{\partial\bar{t}}\bar{P}_{0,i} = \left(\frac{M_PT_0^3G_F^2}{h}\frac{1}{\bar{t}^4}\right)\bar{C}_{0,i} \quad (45)$$
$$\frac{\partial}{\partial\bar{t}}\vec{\bar{P}}_i = \left[-\left(\frac{M_P}{hT_0^3}\bar{\omega}_i\bar{t}^2\right)\hat{B}_V - \left(\frac{M_PT_0^3G_F^2}{h}\frac{\bar{h}_{T,i}}{\bar{t}^4}\right)\vec{B}_{T,i} + \left(\frac{M_PT_0G_F}{h\sqrt{2}\pi^2}\frac{1}{\bar{t}^2}\right)\vec{B}_{L,i}\right]\times\vec{\bar{P}}_i + \left(\frac{M_PT_0^3G_F^2}{h}\frac{1}{\bar{t}^4}\right)\vec{\bar{C}}_i \quad (46)$$

III. RESULTS

In this section, we use the solve_ivp PDE solver from the scipy python library to numerically solve the system of differential equations given in the previous section. We analyze the results in three cases: vacuum Hamiltonian (subsection III B), vacuum Hamiltonian with thermal potential (subsection III C, and vacuum Hamiltonian with thermal and neutrino lepton number potentials (subsection III D). We assume the neutrinos are born electron neutrinos (or antineutrinos) and have a Fermi-Dirac energy distribution:

$$P_{0,i}(\bar{t}=0) = \frac{1}{e^{\bar{E}_i-\bar{\mu}}+1};\quad \vec{P}_i(\bar{t}=0) = \frac{1}{e^{\bar{E}_i-\bar{\mu}}+1}\begin{pmatrix}0\\0\\1\end{pmatrix}$$
$$\bar{P}_{0,i}(\bar{t}=0) = \frac{1}{e^{\bar{E}_i+\bar{\mu}}+1};\quad \vec{\bar{P}}_i(\bar{t}=0) = \frac{1}{e^{\bar{E}_i+\bar{\mu}}+1}\begin{pmatrix}0\\0\\1\end{pmatrix}$$

Where $\bar{\mu} \equiv \mu/T$. Note that omitting the $\vec{B}_L$ term, as is done in subsections III B and III C, we take $\bar{\mu} = 0$. Unless stated otherwise, the mixing angle $\tilde{\theta}$ is taken to be $\tilde{\theta} = \pi/12$; this corresponds to Finally, we take the collision matrix $\bar{g}$ to have components

$$\bar{g}_{ij} = \frac{1}{\bar{E}_1^2}\frac{\bar{E}_j^2}{|\bar{E}_i-\bar{E}_j|+1} \quad (47)$$

A. Vacuum Hamiltonian

For completeness, the solutions for the "pure vacuum" case (i.e., $\partial\vec{P}_i/\partial\bar{t} = (0.2243\times10^{10}\omega_i\bar{t}^2)\hat{B}_V\times\vec{P}_i$) are shown in figure 1. In the absence of thermal and lepton number effects, the effective Hamiltonian vectors $\vec{B}$ and $\vec{\bar{B}}$ maintain a fixed orientation and simply increase in magnitude with $\bar{t}$. $\vec{P}$ and $\vec{\bar{P}}$ therefore precess about $\hat{B}_V$ with increasing angular frequency. With no inelastic collisions, the populations of the energy bins likewise remains static.

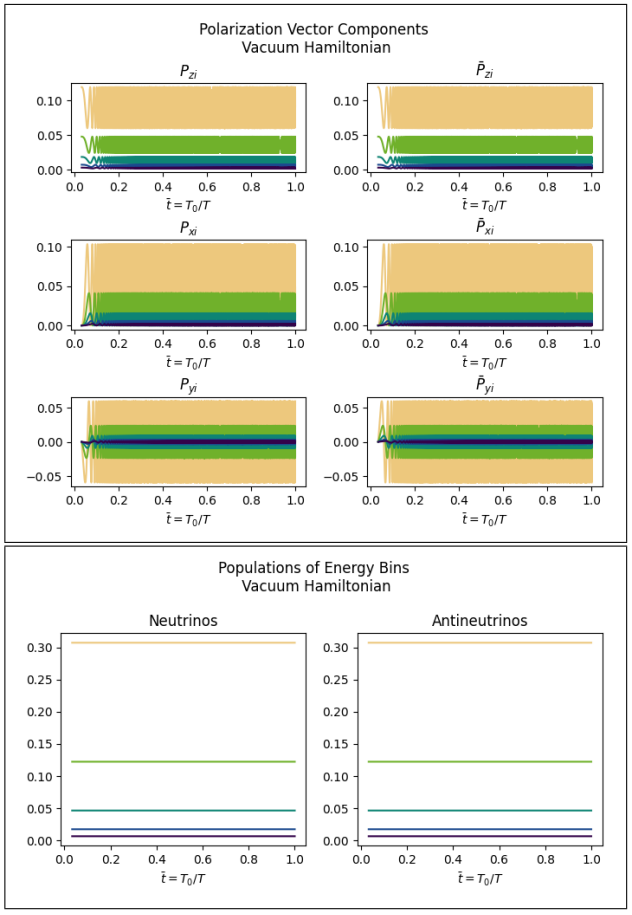

FIG. 1. Components of polarization vectors $\vec{P}$ and $\bar{\vec{P}}$ (above) and normalized "identity component" of polarization vectors $P_{0,i}/Z, \bar{P}_{0,i}/Z$ for $Z = \sum_j P_{0,j} + \bar{P}_{0,j}$ (below) for vacuum Hamiltonian. Different line colors represent different energy bins (violet is higher energy, yellow is lower energy).

B. Vacuum Hamiltonian with Collisions

Now (and from this point onwards) we introduce the inelastic collision terms. Figure 2 shows the components of $\vec{P}$ and $\bar{\vec{P}}$ as a function of $\bar{t}$ for the 5-energy-bin case and for various values of the collision-flavor-dependency parameter δ. In general, increasing δ has the effect of "damping" the oscillations of $\vec{P}$ and $\bar{\vec{P}}$ (with $\delta = 0.5$ showing the "overdamped" case–see figure 3). Figure 3 shows the normalized components of $\vec{P}$ and $\bar{\vec{P}}$ plotted with the normalized components of the effective Hamiltonian vector $\vec{B}$, $\bar{\vec{B}}$ for the same values of δ. In each case, $\vec{P}$ precesses about $\vec{B}$, and the amplitude of this oscillation is damped as $\bar{t}$ increases. $\bar{\vec{P}}$ precesses about $-\bar{\vec{B}}$ in a similar manner. Note that $\vec{P}$ and $\bar{\vec{P}}$ only differ in the y-component, which is consistent with the sign change in the expression for the effective Hamiltonian (i.e., $\vec{P}$ and $\bar{\vec{P}}$ precess along the same axes, but with opposite handedness).

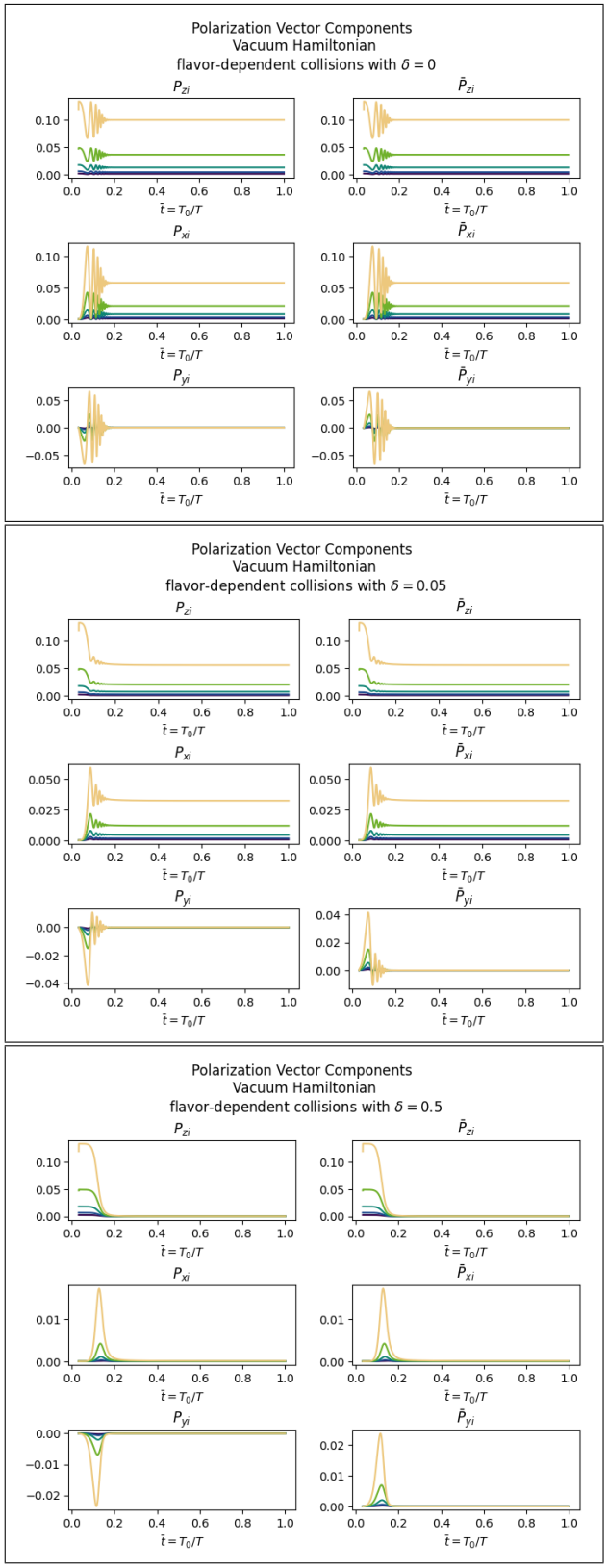

FIG. 2. Components of polarization vectors $\vec{P}$ and $\bar{\vec{P}}$ for several values of flavor-dependency parameter δ (from top to bottom, $\delta = 0, 0.05, 0.5$. Different line colors represent different energy bins (violet is higher energy, yellow is lower energy).

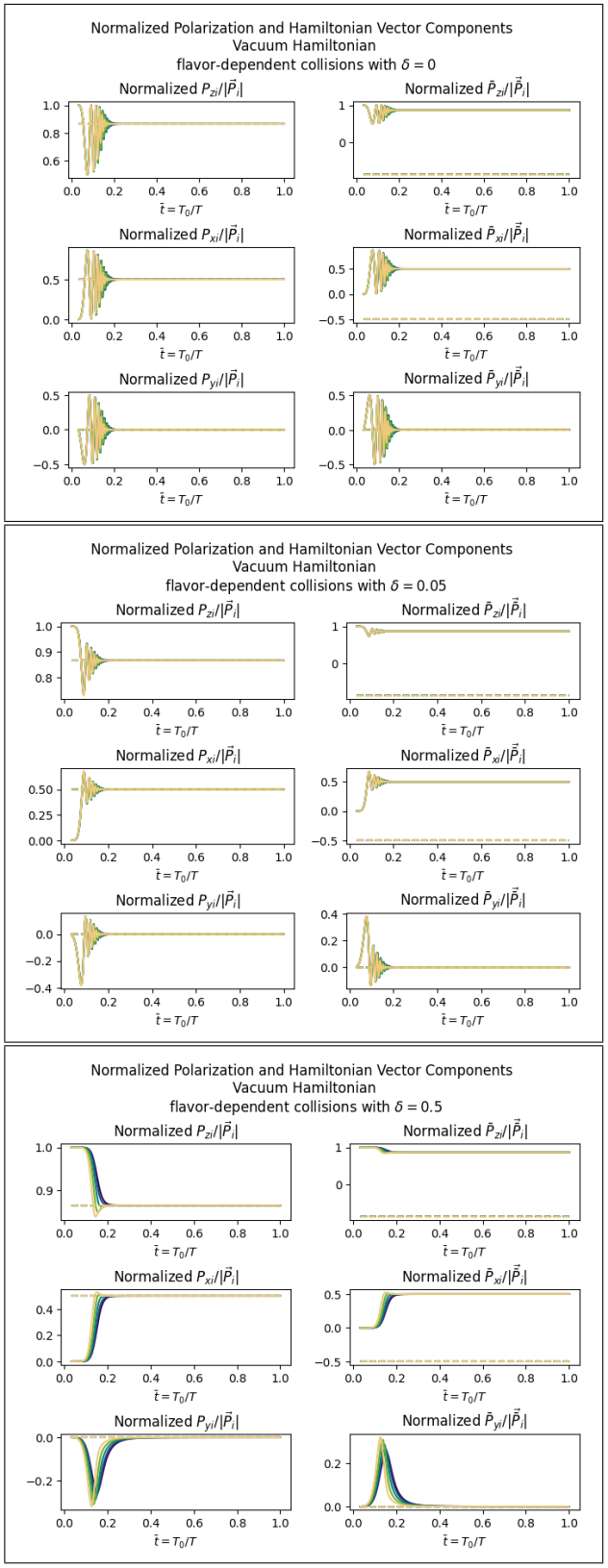

FIG. 3. Normalized components of polarization vectors $\vec{P}/|\vec{P}|, \vec{\bar{P}}/|\vec{\bar{P}}|$ (solid lines) and effective Hamiltonian vectors $\vec{B}/|\vec{B}|, \vec{\bar{B}}/|\vec{\bar{B}}|$ (dashed lines) for several values of flavor-dependency parameter δ (from top to bottom, $\delta = 0, 0.05, 0.5$. Different line colors represent different energy bins (violet is higher energy, yellow is lower energy).

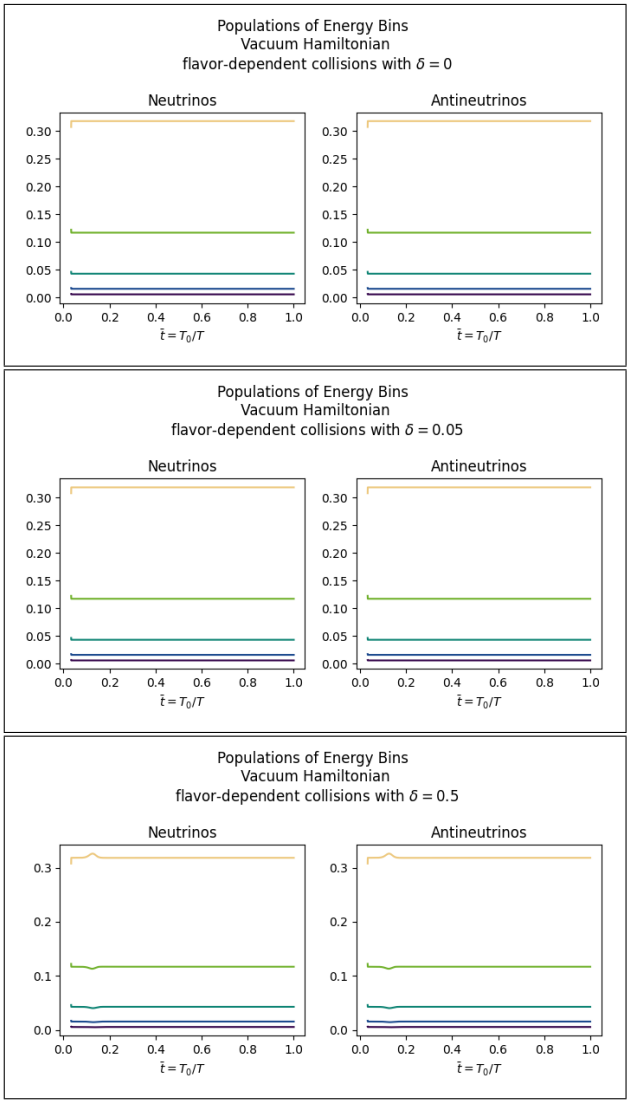

FIG. 4. Normalized "identity component" of polarization vectors $P_{0,i}/Z, \bar{P}_{0,i}/Z$ for $Z = \sum_j P_{0,j} + \bar{P}_{0,j}$ for several values of flavor-dependency parameter δ (from top to bottom, $\delta = 0, 0.05, 0.5$. Different line colors represent different energy bins (violet is higher energy, yellow is lower energy).

Figure 4 shows the normalized populations of the energy bins for neutrinos and antineutrinos ($P_{0,i}$ and $\bar{P}_{0,i}$, respectively) as functions of $\bar{t}$. For small values of δ, the populations remain fixed at the initial Fermi-Dirac conditions. As δ increases, a characteristic "spike" around $\bar{t} \approx 1.5$ becomes more pronounced. This behavior becomes clear when comparing the polarization vector components (figure 2) to the expressions for $C_{0,i}$ and $\bar{C}_{0,i}$ (equation 30). Lower energy polarization vectors initially precess with larger amplitudes but converge faster than higher energies. Increasing δ also causes the different energy bins to converge to smaller (and therefore numerically "closer") amplitudes. If δ is sufficiently large, then the combination of these two effects produces regions where $\sum_{k \neq i} P_{z,i} < e^{\bar{E}_k - \bar{E}_i} P_{z,k}$. This can be seen

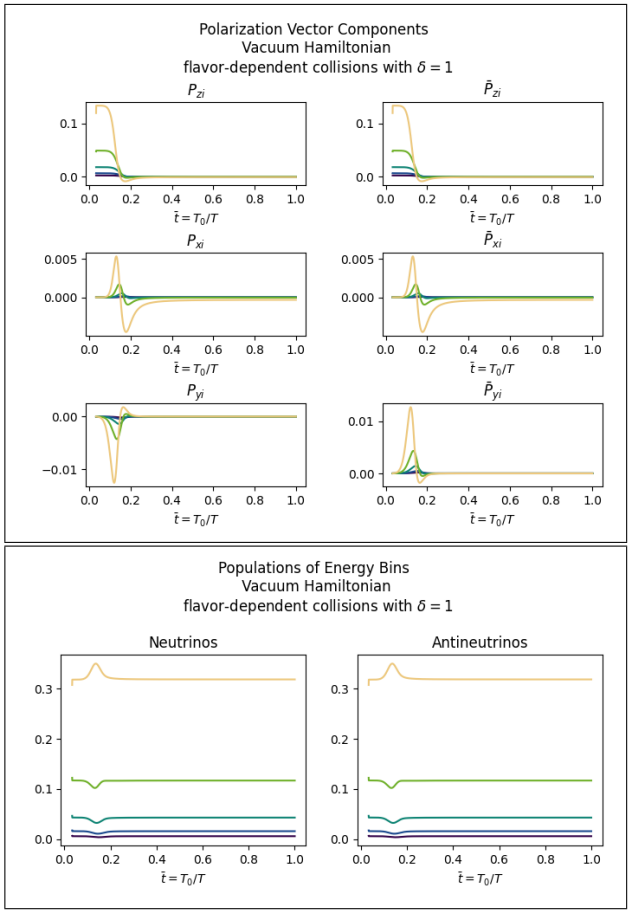

FIG. 5. Components of polization vectors $\vec{P}$ and $\vec{\bar{P}}$ (above) and normalized "identity component" of polarization vectors $P_{0,i}/Z, \bar{P}_{0,i}/Z$ for $Z = \sum_j P_{0,j} + \bar{P}_{0,j}$ (below) for flavor-dependent case $\delta = 1$. Different line colors represent different energy bins (violet is higher energy, yellow is lower energy).

most clearly on the figures for the extreme case $\delta = 1$ (see figure 5), where the lowest energy bin for P_z ($P_{z,1}$, plotted as the yellow line) is suppressed so strongly that there are regions where $P_{z,i} > P_{z,1}$ for $i > 1$ (compare to plots for $\delta = 0$ and 0.05). For these regions, the second term of the expression for $C_{0,i}$ (equation 30) changes, resulting in $\partial_{\bar{t}} P_{0,1} > 0$ and $\partial_{\bar{t}} P_{0,i} < 0$ for $i > 1$. As the values of $P_{0,i}$ change, the first term in $C_{0,i}$ grows in magnitude until it "corrects" for the previous behavior, resulting in the initial distribution being restored.

C. Vacuum Hamiltonian with Thermal Potential and Collisions

In this subsection, we introduce the e^+e^- and $\bar{\nu}\nu$ thermal potentials (equation 28 with scaling given in equation 40) to the terms in the previous section. As with the previous section, figure 6 shows the components for $\vec{P}$ and $\vec{\bar{P}}$ as a function of $\bar{t}$ for various values of δ, and figure 7 shows these same components normalized and plotted with $\vec{B}/|\vec{B}|$ and $\vec{\bar{B}}/|\vec{\bar{B}}|$. With the introduction of the thermal potential, $\vec{B}$ (resp. $\vec{\bar{B}}$) begins aligned with $-\hat{z}$ (resp. $\hat{z}$). Therefore, conversely to what is seen in vacuum, $\vec{P}$ aligns with $-\vec{B}$ and $\vec{\bar{P}}$ aligns with $\vec{\bar{B}}$ (see figure 7).

As with the previous section, increasing δ has the effect of "damping" the polarization vectors, but this effect is not as visually apparent as before. Note that the polarization vectors precess about the effective Hamiltonian vectors, but the amplitude of these oscillations is small enough that they appear to be flat lines when plotted (looking at the output files of the solve_ivp function directly confirms that this is the case).

D. Vacuum Hamiltonian with Thermal and Lepton Potentials and Collisions

Introducing the neutrino lepton number potential was computationally challenging and we ultimately did not succeed in producing solutions for the equations as they are given in equations 43 —46 above. This is primarily due to the limitations of the numerical PDE solver. Given that the neutrino lepton number potential is scaled by a factor of 1.874×10^9 (compared to the scaling of 0.30519 for the thermal potentials), the error tolerances on the PDE solver needed to extraordinarily small to avoid being dominated by noise. However, this forced the program to use time steps $\Delta\bar{t}$ that were so small as to be nonphysical. To proceed, we introduce a scaling factor $\kappa < 1$ to the neutrino lepton potentials:

$$\left(\frac{M_P T_0 G_F}{h\sqrt{2}\pi^2}\frac{1}{\bar{t}^2}\right)\vec{B}_{L,i} \to \kappa\left(\frac{M_P T_0 G_F}{h\sqrt{2}\pi^2}\frac{1}{\bar{t}^2}\right)\vec{B}_{L,i}$$

We proceed by gradually increasing the value of κ and looking at the qualitative trends. The largest value of κ we were able to run was $\kappa = 0.001$.

The neutrino lepton number potential highly suppresses the magnitude of the neutrino and antineutrino polarization vectors–for this reason we will focus on only the normalized components. Figure 9 compares the plots for $\kappa = 10^{-5}$ and $\kappa = 10^{-3}$ for $\bar{\mu} = 1e-3$ in the five energy bin case. For sufficiently large κ, the neutrino lepton number potential dominates and the effective Hamiltonians for neutrinos and antineutrinos are essentially the same (see equations 44 and 46). Thus we no longer have neutrinos and antineutrinos precessing about independent effective Hamiltonian vectors, but, rather, neutrinos and antineutrinos precessing about the same vector in opposite alignment.

A few other general trends are also apparent: First, after an initial period of rapid oscillation, neutrinos emerge aligned with the positive $\hat{z}$-axis while anti-neutrinos emerge aligned with the negative $\hat{z}$-axis. This corresponds to neutrinos decoupling as their original electron-flavor and antineutrinos oscillating to other flavors. This is most clear while looking at the normalized plots (see figures 9 and 10).

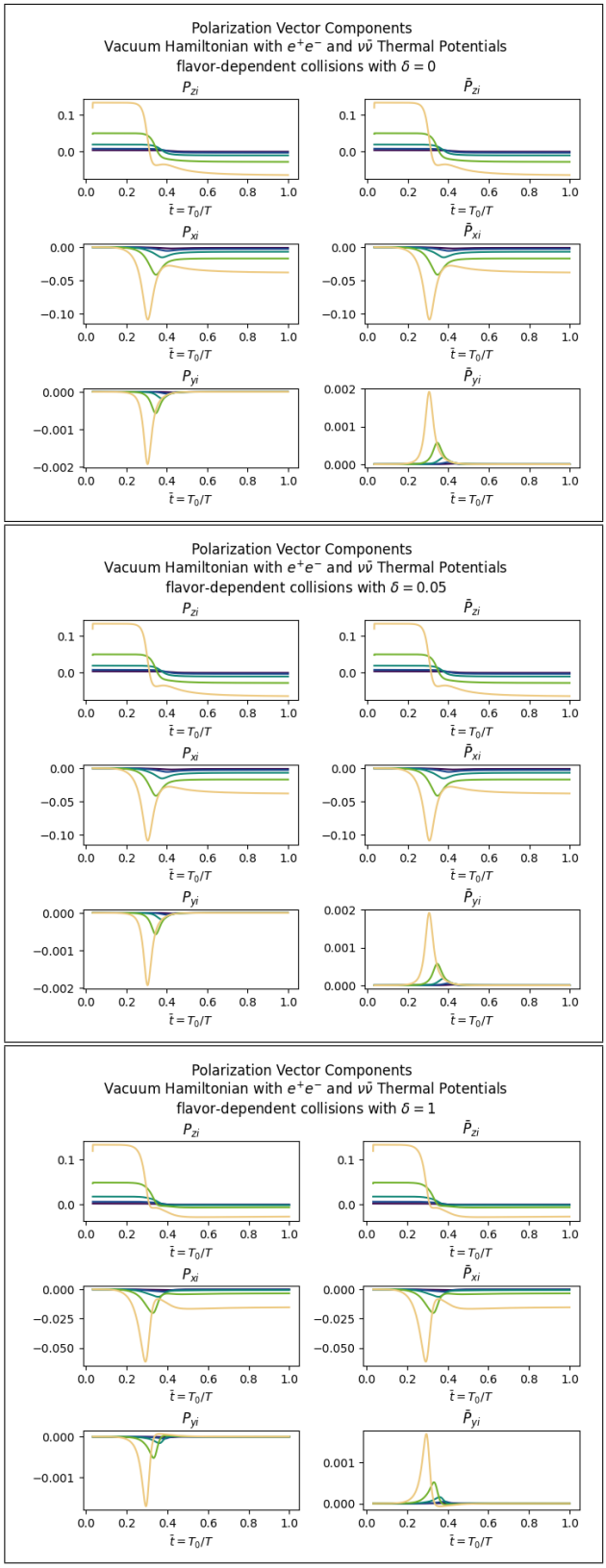

FIG. 6. Components of polarization vectors $\vec{P}$ and $\bar{\vec{P}}$ for several values of flavor-dependency parameter δ (from top to bottom, $\delta = 0, 0.05, 1$. Different line colors represent different energy bins (violet is higher energy, yellow is lower energy).

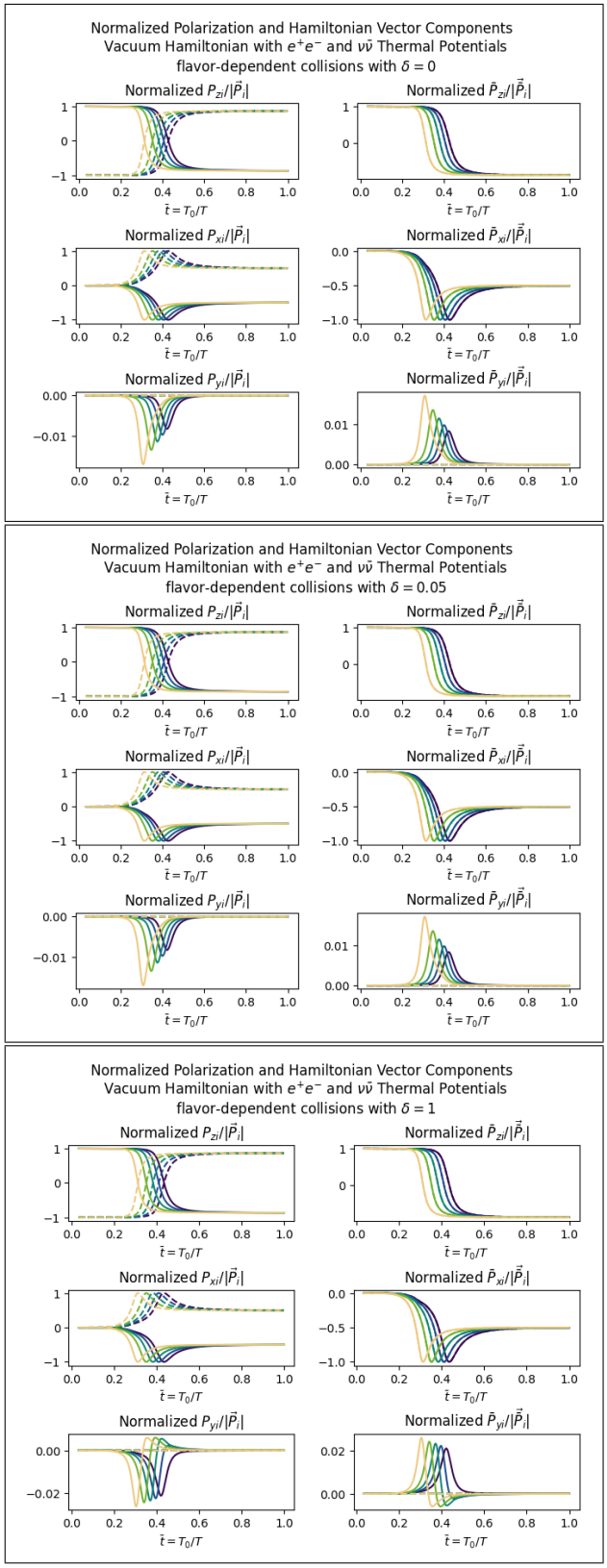

FIG. 7. Normalized components of polarization vectors $\vec{P}/|\vec{P}|, \bar{\vec{P}}/|\bar{\vec{P}}|$ (solid lines) and effective Hamiltonian vectors $\vec{B}/|\vec{B}|, \bar{\vec{B}}/|\bar{\vec{B}}|$ (dashed lines) for several values of flavor-dependency parameter δ (from top to bottom, $\delta = 0, 0.05, 1$. Different line colors represent different energy bins (violet is higher energy, yellow is lower energy).

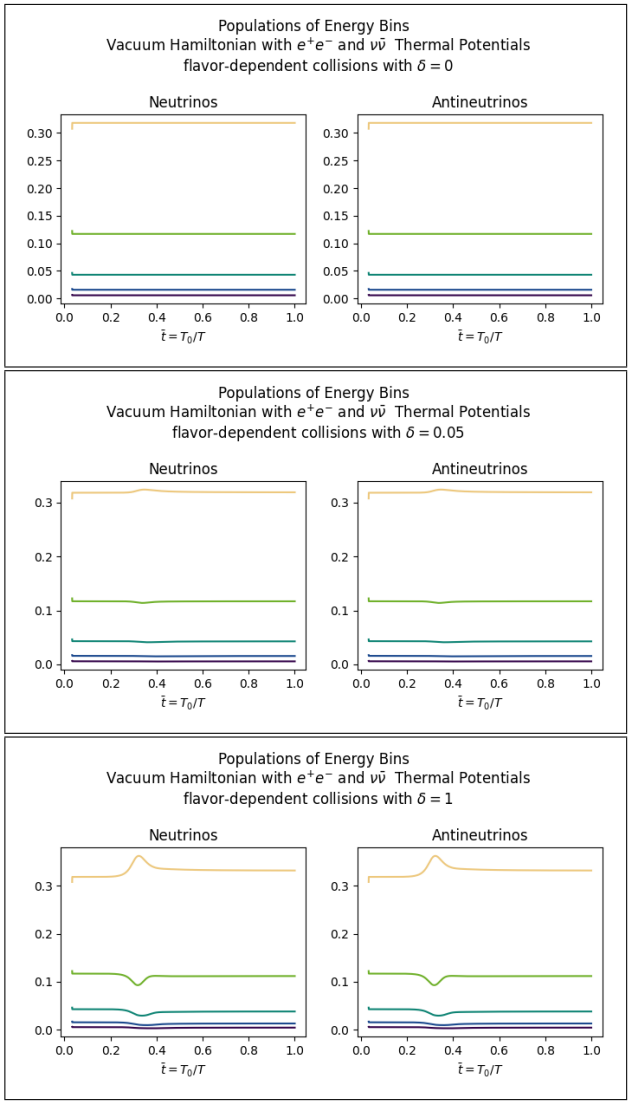

FIG. 8. Normalized "identity component" of polarization vectors $P_{0,i}/Z, \bar{P}_{0,i}/Z$ for $Z = \sum_j P_{0,j} + \bar{P}_{0,j}$ for several values of flavor-dependency parameter δ (from top to bottom, $\delta = 0, 0.05, 1$. Different line colors represent different energy bins (violet is higher energy, yellow is lower energy).

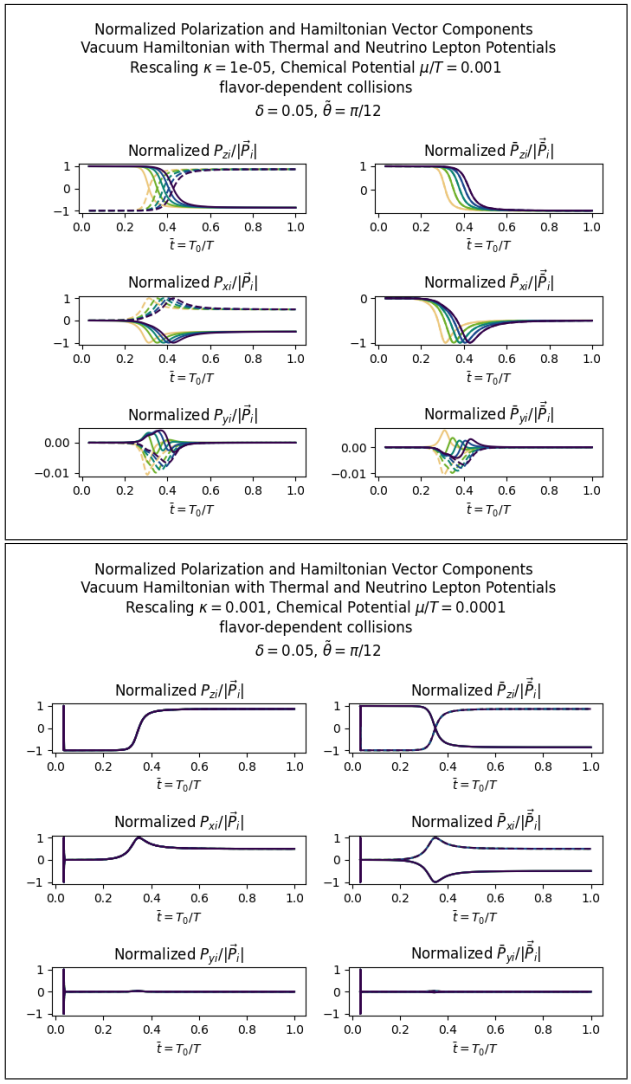

FIG. 9. Normalized components of polarization vectors $\vec{P}/|\vec{P}|, \vec{\bar{P}}/|\vec{\bar{P}}|$ (solid lines) and effective Hamiltonian vectors $\vec{B}/|\vec{B}|, \vec{\bar{B}}/|\vec{\bar{B}}|$ (dashed lines) for several values of rescaling κ (from top to bottom, $\kappa = 10^{-5}, 10^{-3}$. Different line colors represent different energy bins (violet is higher energy, yellow is lower energy).

Second, differences between neutrinos/antineutrinos in distinct energy bins is suppressed. Indeed, in the $\kappa = 10^{-3}$ case one cannot distinguish the plots for the different energy bins in the normalized plots (figure 11 shows details of the non-normalized $\kappa = 10^{-3}$ plots). Note that the energy distribution is still Fermi-dirac; figure 12 shows the normalized P_0 and $\bar{P}_0$ components for the $\kappa = 10^{-3}$ and $\bar{\mu} = 10^{-3}$ case (the plots are identical for other values of $\bar{\mu}$).

Third, the effect of varying $\bar{\mu}$ is rather weak. Figure 10 shows the normalized polarization vector components for $\kappa = 10^{-3}$ and $\bar{\mu} = 10^{-8}$, which may be compared with the $\kappa = 10^{-3}$ and $\bar{\mu} = 10^{-3}$ plot in figure 9. .

Interestingly, this reversal of the neutrino polarization vector is not consistently observed when fewer than five energy bins are used. Figure 13 shows the normalized polarization vector components for the 3 energy bins with $\kappa = 10^{-3}$ and $\bar{\mu} = 10^{-3}$. This plot is interesting for a few reasons: comparing it with figure 10, we see that all components appear to change sign (i.e., it is instead antineutrinos which emerge strongly aligned with the $+\hat{z}$-axis).

IV. DISCUSSION AND CONCLUDING REMARKS

In summary, we have found the following qualitative results:

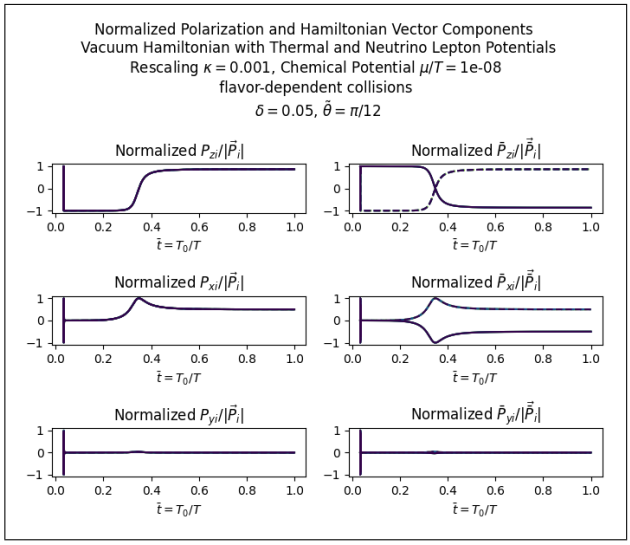

FIG. 10. Normalized components of polarization vectors $\vec{P}/|\vec{P}|, \vec{\tilde{P}}/|\vec{\tilde{P}}|$ (solid lines) and effective Hamiltonian vectors $\vec{B}/|\vec{B}|, \vec{\tilde{B}}/|\vec{\tilde{B}}|$ (dashed lines) for rescaling $\kappa = 10^{-3}$ and chemical potential $\bar{\mu} = 10^{-8}$. Different line colors represent different energy bins (violet is higher energy, yellow is lower energy).

- Inelastic collisions between neutrinos/antineutrinos has the effect of "damping" flavor oscillations. When potential terms are added to the effective Hamiltonian, changing the collision parameter δ (which characterizes flavor-dependency) does not lead to significant qualitative differences.
- Neutrinos and antineutrinos emerge aligned or anti-aligned with the effective Hamiltonian vector (i.e., mass-aligned), which, in tern, is strongly (but not perfectly) aligned with the $\hat{z}$-axis. Thus the mass and flavor eigenstates remain distinct.
- The (rescaled) neutrino lepton number potential induces strong qualitative differences between neutrinos and antineutrinos. Namely, neutrinos emerge strongly aligned with the $+\hat{z}$-axis while antineutrinos emerge strongly aligned with the $-\hat{z}$-axis. This corresponds to neutrinos maintaining their flavor and antineutrinos switching flavor with high probability.
- All interactions and potential terms resulted in the system decoupling in a Fermi-Dirac energy distribution. In the flavor dependent case ($\delta > 0$), this distribution is temporarily disrupted as a result of the Hamiltonian vectors for each energy bin "flipping" at different times.

Perhaps the most remarkable finding is that the neutrino lepton number potential results in the neutrino polarization vectors "flipping" to the positive $\hat{z}$ axis. This behavior is not seen in the absence of the neutrino lepton number potential (except in the vacuum case), nor is it

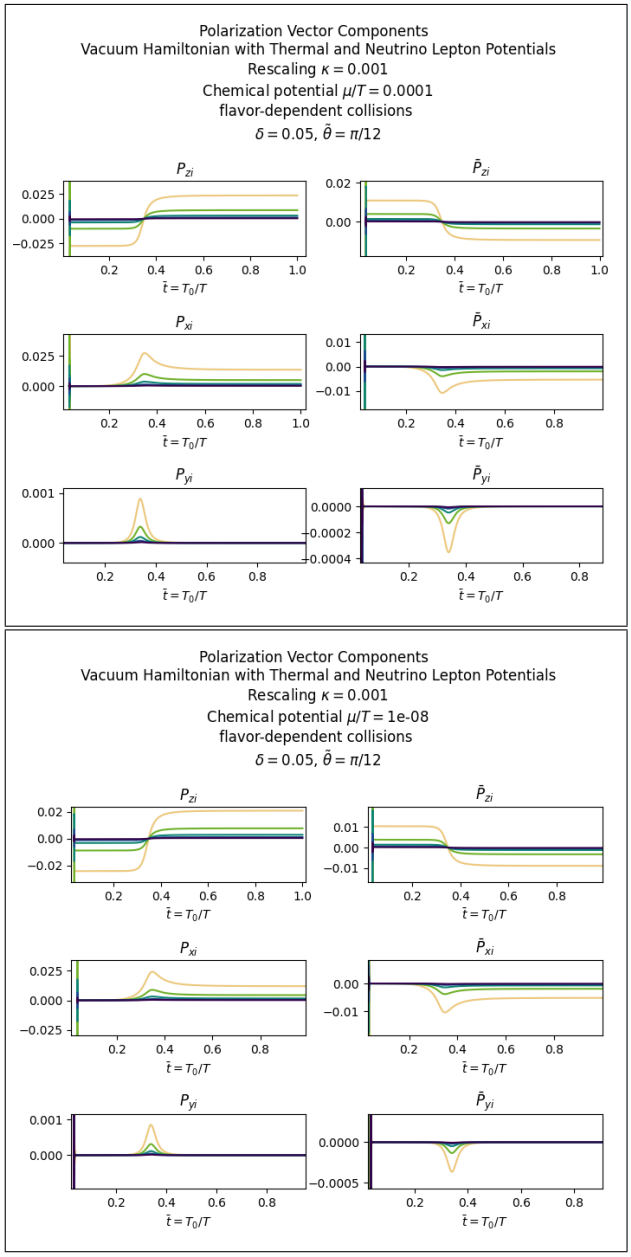

FIG. 11. Detail of components of polarization vectors $\vec{P}/|\vec{P}|, \vec{\tilde{P}}/|\vec{\tilde{P}}|$ (solid lines) and effective Hamiltonian vectors $\vec{B}/|\vec{B}|, \vec{\tilde{B}}/|\vec{\tilde{B}}|$ (dashed lines) for rescaling $\kappa = 10^{-3}$ and chemical potential $\bar{\mu} = 10^{-4}$ (above) and $\bar{\mu} = 10^{-8}$ (below). Different line colors represent different energy bins (violet is higher energy, yellow is lower energy)

consistently observed when fewer than five energy bins are used. Given the technological difficulties with implementing the neutrino lepton potential, we have been unable to diagnose this behavior.

These findings (particularly those relating to the neutrino lepton number potential) would be improved with better technological capabilities. Naturally it would have been ideal to have solutions for the full $\kappa = 1$ scaling. This paper has restricted itself to the $n = 5$ energy bin

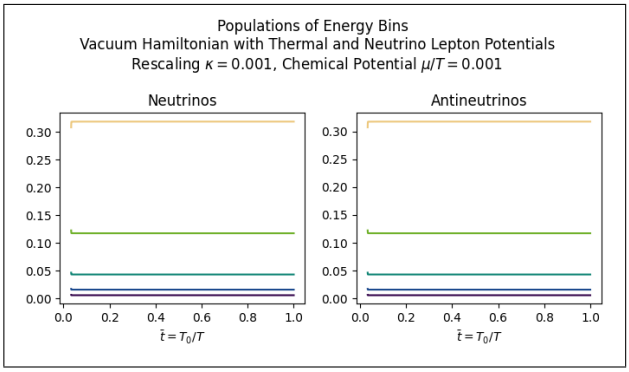

FIG. 12. Normalized "identity component" of polarization vectors $P_{0,i}/Z, \bar{P}_{0,i}/Z$ for $Z = \sum_j P_{0,j} + \bar{P}_{0,j}$ for lepton potential rescaling $\kappa = 10^{-3}$ and chemical potential $\bar{\mu} = 10^{-3}$. Different line colors represent different energy bins (violet is higher energy, yellow is lower energy).

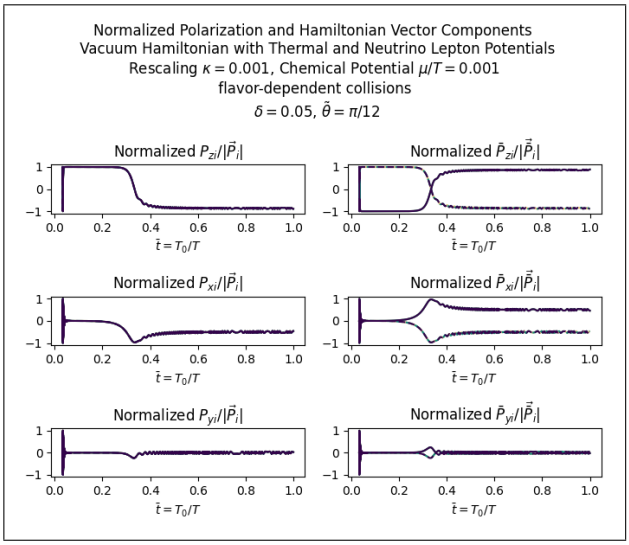

FIG. 13. Normalized components of polarization vectors $\vec{P}/|\vec{P}|, \vec{\bar{P}}/|\vec{\bar{P}}|$ (solid lines) and effective Hamiltonian vectors $\vec{B}/|\vec{B}|, \vec{\bar{B}}/|\vec{\bar{B}}|$ (dashed lines) for 3-energy-bin-case and rescaling $\kappa = 10^{-3}$ and chemical potential $\bar{\mu} = 10^{-3}$. Different line colors represent different energy bins (violet is higher energy, yellow is lower energy).

case; however, in light of our finding that the neutrino lepton number potential exhibits energy-bin-dependent behavior, $n = 5$ is likely not representative of the EU environment.

V. ACKNOWLEDGEMENTS

The authors would like to thank the NSF for sponsoring this research, as well as the University of Washington REU program directors Dr. Gray Rybka and Dr. Arthur Bernard for organizing and running the REU. The lead author would also like to thank Dr. Sanjay Reddy, Dr. Peter Rau, and Dr. Agnieszka Sorensen for their guidance and support throughout the REU program.

[1] C. Giunti and C. W. Kim, *Fundamentals of Neutrino Physics and Astrophysics* (Oxford University Press, 2007).
[2] R. L. Workman and Others (Particle Data Group), Review of Particle Physics, PTEP **2022**, 083C01 (2022).
[3] B. KAYSER, NEUTRINO MASS, MIXING, AND OSCILLATION, in *Flavor Physics for the Millennium* (WORLD SCIENTIFIC, 2001).
[4] J. Linder, Neutrino matter potentials induced by earth (2006), arXiv:hep-ph/0504264 [hep-ph].
[5] A. Y. Smirnov, The msw effect and solar neutrinos (2003), arXiv:hep-ph/0305106 [hep-ph].
[6] R. M. Wald, *General Relativity* (University of Chicago Press, 1984).
[7] S. Dodelson and F. Schmidt, *Modern cosmology*, 2nd ed. (Academic Press, 2021).
[8] M. Taylor, Future stability of expanding spatially homogeneous flrw solutions of the spherically symmetric einstein–massless vlasov system with spatial topology $\mathbb{R}^3$ (2023), arXiv:2306.17774 [gr-qc].